Influence of backside doping on the nonlinear capacitances of a PHEMT affecting the VCO frequency characteristics

H. Brech[†], T. Grave[†], A. Werthof[†], H.-J. Siweris[†], T. Simlinger[‡], and S. Selberherr[‡]

[†]Siemens AG, Corporate Technology, D-81730 Munich, Germany
[‡]Institute for Microelectronics, TU Vienna, Gußhausstraße 27-29, A-1040 Vienna, Austria

Abstract - A local maximum in the $C_{GS}(V_{GS})$ characteristics of an AlGaAs/InGaAs/AlGaAs PHEMT is both calculated by hydrodynamic simulations and extracted from S-parameter measurements. It is found by simulation that the doping on the backside of the channel is the origin of this behavior. VCO measurements demonstrated that this $C_{GS}(V_{GS})$ characteristic can result in a partially reversed tuning behavior.

1. Introduction

High Electron Mobility Transistors (HEMTs) on GaAs substrate are becoming widely used for Microwave Monolithic Integrated Circuits (MMICs) with operating frequencies up to 100 GHz. The most common pseudomorphic HEMT, the AlGaAs/InGaAs/GaAs HEMT without doping below the channel shows high cut-off frequency but low power capability. A second drawback is the high output conductance at short gate lengths. This is a major limiting factor for high frequency performance. However, both power capability and output conductance can be improved by the introduction of a second AlGaAs barrier below the channel which enhances the confinement of the electrons to the quantum well. To improve the power capability, the electron density in the channel is increased by a doping in the AlGaAs buffer. This doping also affects the capacitances of the device.

In the present paper we analyze the mechanisms determining the gate-source capacitance C_{GS} of HEMTs with doping on the backside of the channel. In contrast to HEMTs without backside doping these devices exhibit a local maximum in their $C_{GS}(V_{GS})$ characteristics. Measurements of VCOs employing this type of HEMT [1] show a partially reversed tuning behavior opposite to VCOs with HEMTs without backside doping [2].

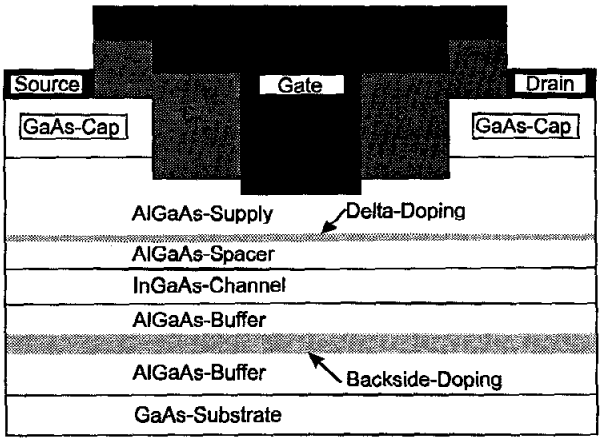

Fig. 1. Schematic cross section of the investigated HEMT.

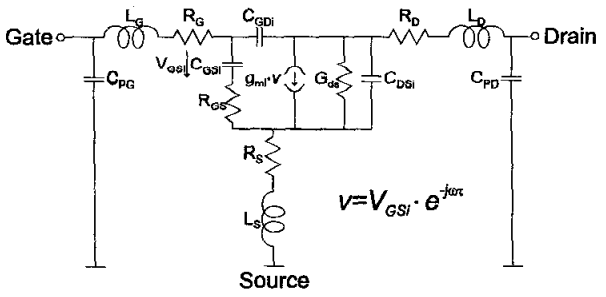

Fig. 2. Small signal equivalent circuit used for parameter extraction.

CCC Code 0-7803-3883-9/98/$10.00 © 1998 IEEE

2. Device structure and simulation

The basic structure of the investigated HEMT is shown in Fig. 1. An InGaAs channel is sandwiched between two AlGaAs barriers. In the barrier below the channel a 5 nm thick layer with a doping concentration of $1.0*10^{18}$ cm^{-3} is used. The upper barrier layer contains a delta doping with a sheet concentration of $3.6*10^{12}$ cm^{-2}. The T-shaped gate with a footprint length l_g of 120 nm was manufactured by optical stepper lithography and a side wall spacer process. Source and drain contacts are self-aligned to the T-gate [1].

The simulations were performed with the hydrodynamic simulator MINIMOS-NT [3]. A hydrodynamic transport model was used in the channel and drift diffusion in the remaining semiconductor layers. The simulation takes into account the complete epitaxial structure, a realistic device topology, i. e., an approximated gate shape, source and drain contacts only on top of the cap layers, and passivation [4].

3. Determination of C_{GS}

The device structure described above enables us to simulate an extrinsic HEMT but without contacting network and pads. The extrinsic gate capacitance $C_{GS}(V_{GS})$ was determined by means of the quasi static approximation

$$C_{GS}(V_{GS},V_{DS}) = \left.\frac{\partial Q_G}{\partial V_{GS}}\right|_{V_{DS}} + \left.\frac{\partial Q_G}{\partial V_{DS}}\right|_{V_{GS}} \tag{1}$$

where Q_G is the total (negative) charge on the gate metal surface. Additionally, small signal parameters were extracted from S-parameter measurements according to [5] using the equivalent circuit shown in Fig. 2. The circuit includes parasitic elements such as pad capacitances and inductances. The quantities determined this way are intrinsic parameters in contrast to the C_{GS} determined by simulation. To compare the intrinsic gate source capacitance C_{GSi} with the simulated extrinsic C_{GS} the following approximation was used

$$C_{GS} \approx (1+g_{mi}R_S)C_{GSi}, \tag{2}$$

where the intrinsic transconductance g_{mi}, the source resistance R_S and C_{GSi} are parameters of the small signal equivalent circuit shown in Fig. 2.

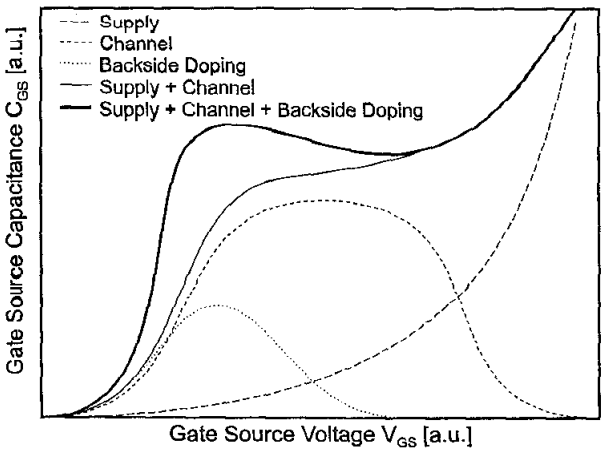

Fig. 3. Contributions to C_{GS} due to backside doping (dots), channel (short dashes) and upper barrier doping (long dashes).

4. Contributions to C_{GS}

The different contributions to C_{GS} are sketched schematically in Fig. 3. In HEMTs with doping only above or in the channel, contributions of channel and upper barrier doping sum up to a well known monotonous increase of C_{GS} with V_{GS}. With an additional doping on the backside of the channel, a third contribution is added. Depending on the doping density and the energy level relative to the channel this can

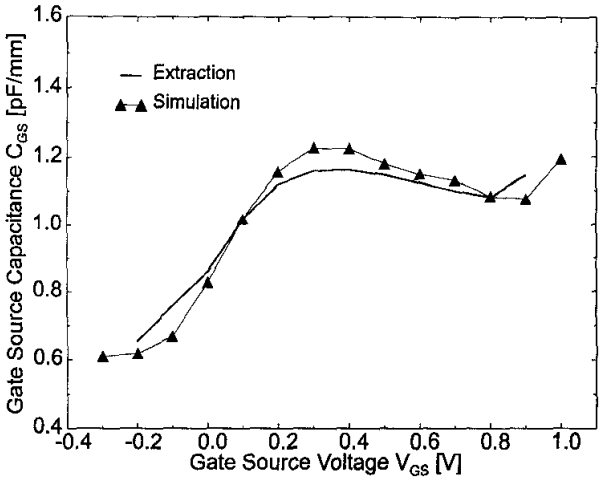

Fig. 4. Simulated and extracted C_{GS} of the investigated HEMT at V_{DS}=3.0 V.

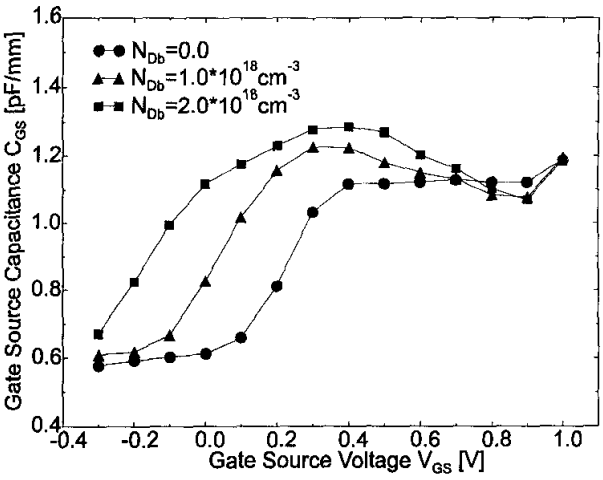

Fig. 5. Simulated C_{GS} of the same HEMT but with different backside doping at V_{DS}=3.0 V.

result in a curve with a local maximum shown by the bold line in Fig. 3.

In Fig. 4, both simulated and extracted $C_{GS}(V_{GS})$ are shown which compare very well. If V_{GS} is increased from pinchoff C_{GS} increases until it reaches a maximum. Both, simulated and extracted C_{GS} show a negative gradient over more than 400 mV of V_{GS} which is the largest part of the usable V_{GS} swing of the device.

Simulations of the same device were performed where only the backside doping N_{Db} was changed. Fig. 5 proves that N_{Db} is the reason for the local maximum of $C_{GS}(V_{GS})$. It demonstrates the dependence of the location and magnitude of the maximum on the concentration of N_{Db}. No local maximum can be observed in the case of $N_{Db} = 0$. With increasing N_{Db}, the pinch off voltage decreases and the local maximum in $C_{GS}(V_{GS})$ appears. The higher the contribution of N_{Db} to the total doping, the more pronounced is the local maximum in the C_{GS} curve. This behavior has an impact on circuits with properties strongly dependent on the $C_{GS}(V_{GS})$ characteristics such as some types of VCOs.

5. VCO characteristics

If a voltage controlled oscillator (VCO) is tuned directly by V_{GS} variations, the change in C_{GS} is one of the most important parameters for its frequency characteristics. Fig. 6 shows a photograph of such

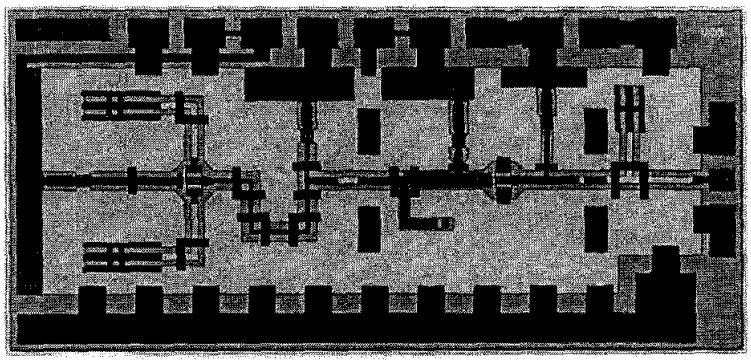

Fig. 6. Layout of the measured VCO.

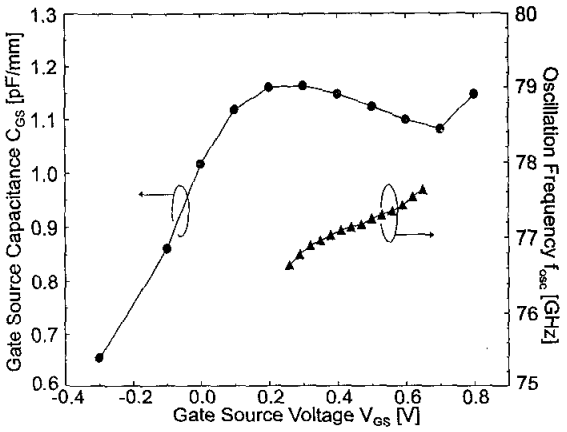

Fig. 7. Measured f_{osc} of the VCO versus the tuning voltage V_{GS} and the extracted C_{GS} of the HEMT used in the VCO.

a monolithic VCO with buffer amplifier [1]. In this type of VCO the output frequency usually decreases with increasing V_{GS} if HEMTs with doping only in or above the channel are employed [2]. This can be different in the same type of VCO if backside doped HEMTs are used [1]. The change in the C_{GS} dependence on V_{GS} due to the backside doping changes the tuning behavior. In particular, the frequency response can be reversed for a certain interval of V_{GS}. Fig. 7 shows the oscillation frequency f_{osc} and the corresponding C_{GS} of the HEMT employed in the VCO, both as a function of V_{GS}. In this case f_{osc} is increasing over the whole range in which the VCO is oscillating. This clearly coincides with the range in which C_{GS} is decreasing with rising V_{GS}. In the case of the measured VCOs no oscillation could be observed for V_{GS} below 0.2 V and above 0.65 V.

6. Conclusion

We have reported a local maximum in the C_{GS} versus V_{GS} characteristics of HEMTs. The same behavior was observed for C_{GS} extracted from S-parameters as well as for C_{GS} obtained from hydrodynamic simulations. We identified the doping on the backside of the channel to be the reason of the local maximum. In agreement with this result we have measured VCO tuning behavior opposite to the one usually observed.

Acknowledgment

The authors would like to thank Dr. H. Tischer for the RF measurements.

References

[1] J.-E. Müller, A. Bangert, T. Grave, M. Kärner, H. Riechert, A. Schäfer, H. Siweris, L. Schleicher, H. Tischer, L. Verweyen, W. Kellner, T. Meier, "A GaAs Chip Set for Automotive Radar Systems Fabricated by Optical Stepper Lithography," *IEEE GaAs IC Symp. Techn. Digest 1996,* pp 189-192.

[2] H. Wang, K. W. Chang, T. H. Chen, K. L. Tan, G. S. Dow, B. Allen, J. Berenz, "Monolithic W-band VCOs using Pseudomorphic AlGaAs/InGaAs/GaAs HEMTs," *IEEE GaAs IC Symp. Techn. Digest 1992*, pp 47-50.

[3] T. Simlinger, H. Brech, T. Grave, and S. Selberherr, "Simulation of Submicron Double-Heterojunction High Electron Mobility Transistors with MINIMOS-NT," *IEEE Transactions on Electron Devices*, Vol. 44, No. 5, pp. 700-707, May 1997.

[4] H. Brech, T. Simlinger, T. Grave, and S. Selberherr, "Current Transport in Double Heterojunction HEMTs," in *ESSDERC'96 - 26th European Solid State Device Research Conference* (G. Baccarani and M. Rudan, eds.), (Gif-sur-Yvette Cedex, France), pp.873-876, Editions Frontiers, 1996.

[5] M. Berroth and R. Bosch, "High-Frequency Equivalent Circuit of GaAs FET's for Large-Signal Applications," *IEEE Trans. on Microwave Theory and Techniques,* VOL. 39, No. 2, pp 47-50, Feb. 1991.